Astron. Astrophys. 352, 228–238 (1999)

ASTRONOMY AND ASTROPHYSICS

Transitional YSOs: candidates from flat-spectrum IRAS sources⋆

E.A. Magnier[1,2], A.W. Volp[2], K. Laan[2], M.E. van den Ancker[2], and L.B.F.M. Waters[2,3]

[1] Astronomy Department 351580, University of Washington, Seattle, WA 98195, USA
[2] Astronomical Institute "Anton Pannekoek", Kruislaan 403, 1098 SJ Amsterdam, The Netherlands
[3] Instituut voor Sterrenkunde, Katholieke Universiteit Leuven, Celestijnenlaan 200B, 3001 Heverlee, Belgium

Received 17 August 1999 / Accepted 5 October 1999

Abstract. We are searching for Young Stellar Objects (YSOs) near the boundary between protostars and pre-main-sequence objects, what we term Transitional YSOs. We have identified a sample of 125 objects as candidate transitional YSOs on the basis of IRAS colors and the optical appearance on POSS plates. We have obtained optical and near-IR imaging of 82 objects accessible from the Northern Hemisphere and optical images of 62 sources accessible from the South. We also created deconvolved 60 μm IRAS images of all sources. We have classified the objects on the basis of their morphology in the optical and near-IR images. We find that the majority of our objects are associated with star-forming regions, confirming our expectation that the bulk of these objects are YSOs. Of the 125 objects, 28 have a variety of characteristics very similar to other transitional YSOs, while another 22 show some of these characteristics. Furthermore we have found seven objects to be good candidates for members of the Herbig Ae/Be stellar group, of which three are newly identified as such. We have placed a set of images for each of the objects in the archives of the Centre de Données astronomique de Strasbourg (CDS).

Key words: stars: circumstellar matter – stars: evolution – stars: formation – stars: mass-loss – stars: pre-main sequence

1. Introduction

The process of individual star formation is usually divided into two important phases. First, the dense core of a molecular cloud collapses to form an embedded protostar which accumulates material by accretion from the surrounding cloud. At some point, the accretion stops, the enshrouding dust is cleared away, and the former protostar, now a pre-main-sequence star, begins to contract slowly, increasing its central temperature until hydrogen ignition takes place. Extensive theoretical and observational work over the past 4 decades has resulted in strong support for this general picture, with most of the major points well understood. One of the areas where uncertainty remains is the transition between the protostar and the pre-main-sequence star. This period is also one of the more interesting in the evolution of the star as the ionized jets and molecular outflows are particularly active at this stage. We are investigating this transitional stage of star formation, and are searching for examples of stars at or near the transition from protostar to pre-main-sequence star. In this paper, we present new optical and infrared imaging observations of a sample of candidate transitional YSOs selected on the basis of IRAS colors and optical morphology. We begin with a background review to motivate our study and the selection criteria of our sample. We then discuss the observations and present our catalog of objects and the relevant observations for each. Finally, we summarize the results of this survey. In successive papers, we will present analyses of the optical and near-IR colors and optical spectroscopy of the best transitional YSO candidates from the sample presented here, as well as submillimeter spectral-line studies.

2. Background

Excellent reviews on the star formation process and the state of the observational evidence have been presented by Stahler (1988b, 1994), Staude & Elsässer (1993), Fukui et al. (1993), and references therein.

The first important attempts to understand the pre-main sequence evolution of stars began in the mid-1950s, with the computer modelling of Henyey et al. (1955), and the identification of T Tauri and Herbig Ae/Be stars (Walker 1956; Herbig 1960). By the early 1970s, the 'standard model' for the evolution of pre-main sequence stars was more or less our modern version, with slow contraction of the star down the Hayashi track followed by a nearly-constant luminosity evolution to the main sequence. While some of the details of this process may have been improved since then, the general picture was already there.

The starting point for pre-main-sequence evolution remained an important theoretical question for the next two decades. Initially it was believed that the details of the cloud collapse were unimportant in determining the temperature and luminosity of the pre-main-sequence star since an insignificant fraction of the gravitational potential energy would be lost in the collapse. Later work showed that large amounts of energy are dissipated in the accretion, implying that the details of the

Send offprint requests to: Eugene A. Magnier

⋆ Based on observations collected at the European Southern Observatory, La Silla, Chile.

Correspondence to: gene@pikake.astro.washington.edu

collapse were important in determining the starting point of the pre-main-sequence evolution. Further theoretical work by Shu (1977) demonstrated the 'inside-out' collapse process which resulted from the nearly isothermal nature of the dense cloud core.

Further work to model the protostar collapse resulted in the first believable starting point for the pre-main-sequence evolution. Stahler (1983; 1988a) suggested that pre-main-sequence stars should first be seen in a narrow locus, the "birthline", determined by the mass-radius relationship of the protostar during the final, deuterium-burning stage. Contemporary observational evidence from pre-main-sequence stars supported this claim (Cohen & Kuhi 1979).

By the early 1980s, the existence of embedded, accreting protostars was widely believed, but observational evidence was limited. Dense cloud cores had been observed in studies of molecular gas (Myers & Benson 1983). Lada & Wilking (1984) studied the spectral energy distribution of the infrared sources in Ophiuchus and grouped the sources into three classes. Class I sources consisted of rising infrared spectral energy distributions and were nearly always unidentified at optical wavelengths. Class II sources consisted of T Tauri stars with flat or slightly falling infrared spectral energy distributions. Class III objects were consistent with reddened blackbody spectra. They equated Class III objects with main-sequence and pre-main-sequence stars with small amounts of extinction, Class II objects with pre-main-sequence stars with moderate amounts of warm dust, and Class I objects with protostars. Adams & Shu (1986, 1985) and Adams et al. (1987) developed models for the spectral energy distributions of these systems and strengthened the connection between the sequence of Class I, Class II, Class III and the above evolutionary sequence.

2.1. Disks and outflows

The work discussed above has resulted in a generally accepted scenario for the formation and evolution of the central star, but it is lacking in two major areas: the presence of disks and outflows. While the presence of disks was predicted in theories, observational evidence for disks was slow to develop. Conversely, collimated outflows were not predicted in early theories, but observational evidence existed for many years: Optical spectra of T Tauri stars showed early on the presence of strong winds (Joy 1945; Herbig 1960; Kuhi 1964). Luyten (1971) pointed out the large proper motion of Herbig-Haro objects associated with L1551. Several groups explained HH objects as the result of wind-cloud interactions (Schwartz 1978; Norman & Silk 1979; Rodriguez et al. 1980). Cudworth & Herbig (1979) confirmed the Luyten (1971) result and made several suggestions for the proper motion, including the suggestion that the objects were moving away from the position of the infrared source L1551 IRS 5. The real breakthrough came with the discovery of Snell et al. (1980) of a bipolar CO outflow from L1551 IRS 5. In this classic paper, they presented all of the modern components of an accreting YSO system: large lobes of the molecular outflow driven by a fast, ionized wind collimated by a thick torus of material surrounding the central star.

At about the same time that outflows were recognized, evidence was mounting for the presence of disks in YSO systems. The spectral energy distribution models of Adams & Shu (1985) implied the presence of warm circumstellar disks to explain the amount mid-IR emission. The large observed amounts of mid and far-IR emission in systems with relatively low extinction to the central star also imply a large amount of warm dust in a disk geometry. Several systems such as L1551 IRS 5 and R Mon show evidence for disks in the axisymmetric pattern of light reflected off nearby reflection nebulae. The shape of emission line profiles in which blue-shifted wings are preferentially seen are further evidence of obscuring circumstellar disks (e.g., Mundt 1984). Recently, disks have been directly imaged, via their IR emission (e.g., Beckwith et al. 1989, Chen et al. 1998), and with HST via the absorption of the background emission (McCaughrean & O'Dell 1996).

Disks may be present in YSO systems in a variety of shapes and sizes. On the largest scales, the envelope of molecular gas may be rotating slowly around the central object. Evidence for such large scale (1000–10 000 AU) bulk motions has been seen in the CO velocity fields for several embedded YSOs (see Staude & Elsässer 1993 for a review). The disks which have been imaged directly had diameters in the range of 10s–100s of AU and consist largely of warm dust. Finally, on the smallest scales, accretion is thought to take place from the hot boundary layer of an accretion disk with scales of only a few stellar radii. The presence of UV excesses and strong high-Balmer line emission in active systems are thought to be evidence for hot accretion disks (see e.g. Batalha & Basri 1993), though other models have been suggested in the literature.

2.2. YSOs in transition

One of the most important issues in the formation of young stars is the end of accretion. The point at which accretion stops determines the mass of the star which will develop. The mechanism which interrupts the accretion process is not well understood, but one likely possibility is that the presence of a strong outflow may disrupt the cloud. During this period, outflow activity is usually quite strong. The end of accretion approximately marks the transition between the embedded and exposed phases of evolution. The transition between these two stages is apparently quite quick, as seen in the dichotomy between Class I sources and Class II sources: there are few sources with very flat far-IR SEDs. It is difficult to study the sources which are close to this transition as they tend to have substantial extinction to the central star, making optical observations difficult or impossible. Certain systems which are close to this boundary, such as L1551 IRS 5, may be observed optically only via a reflection off of a nearby dusty cloud.

IRAS 05327+3404, first discussed in depth by Magnier et al. (1996; Paper I), is an excellent example of a YSO in transition. IRAS 05327+3404 (Holoea) has some features typical of Class I sources (rising spectral energy distribution, molecular bipolar

outflow) and some features typical of Class II sources (visible central star, ionized outflow). Furthermore, the outflow is of an unusually high velocity ($\sim$650 km s^{-1}) for a low-mass star (roughly K1), and the central star has brightened by > 1.5 magnitudes since the 1954 POSS plates. All of these pieces of evidence suggest that this source is not only close to the Class I / Class II (Lada & Wilking 1984) boundary, but in fact in the process of becoming optically exposed. IRAS 05327+3404 (Holoea) clearly represents a unique opportunity to study an optically visible low-mass star which retains substantial circumstellar material.

There are other well-studied systems, such as L1551 IRS 5 and Parsamyan 21, consisting of low-mass stars which must also be close to the Class I / Class II transition, but which are more embedded than IRAS 05327+3404 (Holoea) and have substantially higher extinctions. Other objects with nearly flat IRAS spectra, such as DG Tau and T Tau, are close to the boundary, but have substantially less mid- and far-IR emission than IRAS 05327+3404 (Holoea). The object HL Tau is probably at a very similar state of evolution, and it shows an SED very similar to that of IRAS 05327+3404 (Holoea). We have searched for more examples of objects near the embedded/exposed transition by searching for objects with properties similar to IRAS 05327+3404 (Holoea).

3. Candidate selection

Our goal is to find objects near the transition between the embedded and exposed phases of evolution. Such sources will naturally have generally flat IRAS spectra, and will likely exhibit some of the properties of other sources thought to be near the transitional phase, such as strong ionized and molecular outflows, nearby reflection nebulae, moderate to high optical extinction. Similar searches have been performed in the past by researchers who selected candidate YSOs from the IRAS Point Source Catalog (1985) by identifying objects with IRAS colors similar to known YSOs (e.g., Persson & Campbell 1987; Campbell et al. 1989; Prusti et al. 1992). In this project, we have used the source IRAS 05327+3434 (Holoea) as a guideline. We are searching for sources which resemble this source, starting with the IRAS colors.

We have selected candidate transitional YSOs from the IRAS Point Source Catalog (1985) based on their IRAS colors. IRAS colors may be defined as logarithmic flux ratios, e.g., $[12] - [25] = -2.5 \log(\frac{f_{12}}{f25})$. We used the IRAS $[12] - [25]$, $[25] - [60]$ color-color diagram to make the initial selection of candidates. We based our selection partly on the IRAS colors of Holoea and partly on the colors of a perfectly flat IRAS spectrum. We chose all sources in the $[12] - [25]$, $[25] - [60]$ color-color diagram within a specific box. We chose the center of our box to have the $[12] - [25]$ color of a flat IRAS source ($[12] - [25] = 0.75$), while the $[25] - [60]$ center was chosen as the color of Holoea ($[25] - [60] = 1.5$). The width of the box was chosen to be roughly 2σ for each color, giving us the following color ranges: $1.3 < [12] - [25] < 0.40, 2.0 < [25] - [60] < 1.0$. We also demanded that all IRAS sources have a good detection with reliable data (Category 3 detection) in the bands 12 μm, 25 μm, and 60 μm. These criteria resulted in 327 IRAS sources.

To narrow down the list, we examined the Digitized Palomar Observatory Sky Survey (DSS) in the vicinity of each source. We extracted small ($4' \times 4'$) images around each source and searched for any hint of nebulosity. Since the reflection nebula of Holoea is quite faint in the DSS images, we did not demand a very significant level of nebulosity for the new candidates. Since the nuclei of Seyfert galaxies may have IRAS colors similar to our selected range, a number of sources which were clearly associated with spiral galaxies were also rejected. These criteria reduced our initial sample to a manageable selection of 125 sources. Table 1 lists the entire sample of sources in the final selection. In this paper, we report on imaging observations of the sources. We present optical, near-IR and deconvolved IRAS images (HIRAS) of each source, available in electronic form only.

4. Observations

Observations of the Southern sources were performed using the Dutch 90cm telescope at the European Southern Observatory, La Silla. Observations have been made in June 1996 by S. Kramer, in September 1996 by T. Thomas, in December 1996 by D. Janssens, in January 1997 by H. Sellmeijer, and in August 1998 by J. Arts. The Dutch telescope is equipped with a TEK 512^2 CCD with a pixel scale of about $0\farcs44$. Bessel V (λ_c = 5442 Å, FWHM = 1171 Å), Bessel R (λ_c = 6481 Å, FWHM = 1645 Å), and Gunn i (λ_c = 7972 Å, FWHM = 1407 Å) have been used. Exposure times were 5 minutes per image. All sources have been imaged three times in each filter. These three exposures were then averaged, during which outliers caused by cosmic ray impacts on the CCD were rejected. Images were then bias subtracted and flat-field corrected. Positional calibration was done by identifying field stars using DSS images.

Observations of the Northern Hemisphere sample were performed using the Apache Point Observatory (APO) 3.5m telescope. Observations were distributed over a number of nights between Aug 1996 and Feb 1998. Table 2 lists the nights of observations and the instruments used. Observations were made using three different instruments. The APO 3.5m was remotely operated from the University of Washington control room for all of the observations. The Apache Point Observatory has a mid-IR all-sky imager which operates at 10 μm and observed the entire sky once every 5 to 10 minutes. This camera, the CloudCam allows the observer to directly see the presence of even quite low levels of cirrus clouds, making it possible to judge the conditions as the night progresses. The photometric conditions of the sky during each of the nights are listed in Table 2. Consistency of the standard star photometry during the photometric nights was used to judge the accuracy of the photometric calibrations. Although not all of the nights of observation were photometric, good calibrations for nearly all Northern sources were determined during the photometric nights. Calibrated photometry for individual objects will be presented in a follow-up paper.

Table 1. Transitional YSO candidate IRAS sources

IRAS ID	RA (J2000) DEC	g'	r'	i'	g	r	V	R	I	J	H	K	ID	notes
00294+6510	00 32 18.5 +65 27 19	●	●	●	●	●	×	×	×	●	●	●	1	1 v. red star, bright neighbour, refl. neb.
00353+6249	00 38 17.1 +63 06 01	●	●	●	●	●	×	×	×	●	●	●	1	1 v. red star, refl. neb.
00544+5609	00 57 26.1 +56 25 16	×	×	×	●	●	×	×	×	●	×	●	5	reddened cluster
02048+5957	02 08 27.0 +60 11 45	×	×	×	●	●	×	×	×	●	×	●	5	reddened cluster
02259+7246	02 30 43.8 +72 59 39	●	×	●	●	●	×	×	×	●	●	●	2	*in L1340*, faint red star, refl. neb.
03260+3111	03 29 10.4 +31 21 58	●	×	●	●	●	×	×	×	●	●	●	1	*in NGC 1333*, v. red star, lots of refl. neb.
03383+4343	03 41 44.8 +43 52 54	●	●	●	●	●	×	×	×	●	●	●	1	red star, some neb.
03412+6759	03 46 08.7 +68 09 05	●	×	●	●	●	×	×	×	●	●	●	6	*in IC 342*, H II region in spiral galaxy arm
03507+3801	03 54 05.5 +38 10 39	●	×	●	●	●	×	×	×	●	●	●	1	*by refl. neb. PP 11*, red star
04020+5017	04 05 47.0 +50 25 07	●	●	●	×	×	×	×	×	●	●	●	2	several (2-3) m. red stars, no obv. neb.
04038+5437	04 07 50.1 +54 45 33	●	●	●	×	×	×	×	×	●	●	●	2	several (2-3) m. red stars, no obv. neb.
04104+5029	04 14 14.9 +50 37 25	●	●	●	●	●	×	×	×	●	×	●	5	m. red group of stars
04115+5027	04 15 22.2 +50 34 37	●	●	●	●	●	×	×	×	●	×	●	1	v. red star, several m. red stars
04278+2435	04 30 52.7 +24 41 49	●	×	●	×	×	×	×	×	●	×	●	2	**ZZ Tau YSO**, by mol. cl. OMK96 30, 1 m. red star
04287+1807	04 31 38.8 +18 13 56	●	●	●	●	●	×	×	×	●	×	●	3	**HL Tau YSO**, *in L1551*, 2 v. red stars, emis. + dark neb.
04362+4913	04 40 02.5 +49 18 52	●	●	●	●	●	×	×	×	●	×	●	6	**ZOAG 156.16+01.78**, highly extinguished galaxy
04553−6921	04 55 05.3 −69 16 55	×	×	×	×	×	●	●	●	×	×	×	1	*in LMC*, some neb., busy field
05017+2639	05 04 50.6 +26 43 18	●	×	●	×	×	×	×	×	●	×	●	4	**HD 32509**, bright star, some faint neb. HAeBe?
05044−0325	05 06 55.7 −03 21 12	●	×	●	×	×	●	●	●	●	×	●	3	**NSV 1832**, *by L1616 in NGC 1788*, several stars in neb.
05111+3244	05 14 24.7 +32 47 57	●	×	●	●	●	×	×	×	●	×	●	3	**HD 241699**, 2 v. red stars, other m. red stars, HAeBe?
05177+3636	05 21 09.3 +36 39 34	●	×	●	×	×	×	×	×	●	×	●	3	2 red stars + neb.
05198+3325	05 23 08.3 +33 28 36	●	●	●	●	●	×	×	×	●	×	●	3	**CPM 16 YSO**,*in NGC 1893, by S236*, red stars, emis. neb.
05223+1908	05 25 16.3 +19 10 45	●	×	●	×	×	×	×	×	●	×	●	2	1 red star, some neb.
05235+4033	05 27 03.9 +40 35 40	●	●	●	●	●	×	×	×	●	×	●	5	*in S225*, some neb.
05293+1701	05 32 14.2 +17 03 25	●	×	●	×	×	×	×	×	●	×	●	4	**HD 36408**, pair of bright stars, highly sat.
05318+2749	05 34 56.8 +27 50 58	●	×	●	×	×	×	×	×	●	×	×	3	pos. dark neb., 2 v. red stars, 1 m. red, some neb.
05327+3404	05 36 05.4 +34 06 11	●	×	●	×	×	×	×	×	●	×	●	1	**Holoea!**, *in M36, NGC 1960*, v. red star + refl. neb.
05341−0610	05 36 36.0 −06 08 24	●	×	●	×	×	●	●	●	●	×	●	7	Nothing obvious
05343+3605	05 37 41.8 +36 07 20	●	●	●	●	●	×	×	×	●	×	●	2	*by S233, S231*, several m. red stars, 1 v. red + neb.
05364−0722	05 38 51.2 −07 21 05	●	×	●	×	×	●	●	●	●	×	●	3	**Haro 4-254 YSO**, *in L1641*, 2-3 red stars, dark + emis neb
05373+2349	05 40 24.5 +23 50 53	●	×	●	×	×	×	×	×	●	×	●	1	**CPM 19 YSO**,*in KOY98 81* 1 v. red star
05437+2502	05 46 51.6 +25 03 44	●	●	●	●	●	×	×	×	●	×	●	6	**CAP 0543+25**
05440+2059	05 47 02.2 +21 00 10	●	×	●	×	×	×	×	×	●	×	●	5	*in CB88 34* several red stars in group
05482+0306	05 50 53.3 +03 07 41	●	×	●	●	●	●	●	●	●	×	●	3	**RNO 57 (HH Obj.)**,*in L1617*, 1 v. red, 2 m. red, much neb.
05555−1405	05 57 49.6 −14 05 41	×	×	×	●	●	●	●	●	●	×	●	5	*in vdB 64*, several red stars in group?
06005+3010	06 03 43.5 +30 10 16	●	×	●	×	×	×	×	×	●	×	●	5	*by S241, in LBN 825*, several red stars, 1 v. red
06017+3006	06 04 57.1 +30 06 40	●	●	●	●	●	×	×	×	●	×	●	5	*by S241*, some red stars
06040+2958	06 07 16.1 +29 58 00	●	●	●	●	●	×	×	×	●	×	●	5	**CPM P3 YSO, P85b 4** one red clump, faint red stars
06041+3012	06 07 23.8 +30 11 44	●	●	●	×	×	×	×	×	●	×	●	2	**MWC 790 HAeBe?**1 v. red star, is cluster?
06047−1117	06 07 08.3 −11 17 51	●	×	●	×	×	●	●	●	●	×	●	1	a v. red star + neb. (emis?)
06059−0935	06 08 20.7 −09 36 03	●	×	●	×	×	●	●	●	●	×	●	3	2-3 red stars, neb. multi-HIRAS source
06134+2348	06 16 32.8 +23 47 22	●	●	●	×	×	×	×	×	●	×	●	5	**ZOAG 187.90+03.46 (mis-ID?)**, v. red group in IR
06142+1439	06 17 04.6 +14 37 51	●	×	●	×	×	×	●	●	●	×	●	5	*by S267*, red group, some fuzz in opt
06244+0336	06 27 02.5 + 3 34 21	●	×	●	×	×	●	●	●	●	×	●	1	v. red star
06303+1021	06 33 04.4 +10 19 20	●	×	●	×	×	●	●	●	●	×	●	4	**NGC 2247 nebula**, sat in g, i, J, K. neb?
06323+0718	06 35 01.3 +07 15 57	●	×	●	×	×	●	●	●	●	×	●	5	m. red clump of stars
06351−0055	06 37 42.2 −00 58 36	×	×	×	×	×	●	●	●	×	×	×	7	**CPM 28**,*by S283*, globules on DSS?
06384+0932	06 41 11.0 +09 29 31	●	×	●	×	×	●	●	●	●	×	●	3	**NGC 2264 IRS 1 yso**, *by S273*, 2-3 v. red stars, lots of neb.
06502−0040	06 52 45.0 −00 43 56	×	×	×	×	×	●	●	●	×	×	×	7	**ZOAG 213.73-00.04 (mis-ID?)** nothing obvious
06522−0350	06 54 45.0 −03 54 18	●	×	●	×	×	●	●	●	●	×	●	3	**ZOAG 216.79-01.04 (mis-ID?)**, *in G216-2.5*, red stars, neb
06535+0037	06 56 06.0 +00 33 51	●	×	●	×	×	●	●	●	×	×	×	2	**CPM 31 YSO, ZOAG 212.96+01.29**, m. red star, neb
06547−0105	06 57 17.9 −01 09 48	●	×	●	×	×	●	●	●	×	×	×	7	*in FT96 214.7+0.7*, nothing obvious
06548−0815	06 57 14.7 −08 19 54	×	×	×	×	×	●	●	●	×	×	×	3	**BFS 63**,*in FT96 220.9-2.5*, red stars, neb.
06567−0350	06 59 14.5 −03 54 51	×	×	×	×	×	●	●	●	×	×	×	1	**BFS 56**,*in FT96 217.4-0.1* v. red star, neb.
06568−1154	06 59 13.0 −11 58 56	×	×	×	×	×	●	●	●	×	×	×	1	**CMa West**

● = data obtained; × = data not obtained

Table 1. (continued)

IRAS ID	RA (J2000) DEC	g'	r'	i'	g	r	V	R	I	J	H	K	ID	notes
06584−0852	07 00 51.6 −08 56 28	×	×	×	×	×	•	•	•	×	×	×	1	**CPM 33 YSO**,*in FT96 221.9-2.0*, red stars, neb.
07166−1816	07 18 50.8 −18 22 11	×	×	×	×	×	•	•	•	×	×	×	2	some neb.
07183−2741	07 20 21.1 −27 47 02	×	×	×	×	×	•	×	•	×	×	×	2	**Bran 19**,1 red star, some neb.
07221−2544	07 24 13.6 −25 50 03	×	×	×	×	×	•	•	•	×	×	×	2	*in Bran 23*,1 red star, some neb. (emis?)
07254−2259	07 27 35.0 −23 05 25	×	×	×	×	×	•	•	•	×	×	×	2	some neb.
07466−2631	07 48 43.4 −26 39 29	×	×	×	×	×	•	•	•	×	×	×	2	some neb., spike from HD 63599
08100−3818	08 11 55.1 −38 27 54	×	×	×	×	×	•	•	•	×	×	×	7	nothing obvious
08211−4158	08 22 52.3 −42 07 56	×	×	×	×	×	•	•	•	×	×	×	1	**HH obj**,*in vdB 15*, refl. neb.
08404−4033	08 42 17.1 −40 44 10	×	×	×	×	×	•	•	•	×	×	×	2	**ESO Hα 162**,*in BRAN 174*, refl. neb.
08474−4649	08 49 07.7 −47 00 23	×	×	×	×	×	•	•	•	×	×	×	3	*in BRAN 187*,3 red stars, ringlike neb.
08500−4254	08 51 49.2 −43 05 30	×	×	×	×	×	•	•	•	×	×	×	2	*in star forming region?*, red star, some faint neb.
08534−4301	08 55 13.9 −43 12 57	×	×	×	×	×	•	•	•	×	×	×	7	*in GUM 19?*, nothing obvious
09207−4757	09 22 30.8 −48 10 08	×	×	×	×	×	•	•	•	×	×	×	7	*in BRAN 259*, nothing obvious
10075−6647	10 08 50.5 −67 01 52	×	×	×	×	×	×	×	×	×	×	×	6	**IC 2554 galaxy**
10207+2007	10 23 30.4 +19 51 54	×	×	×	×	×	×	×	×	•	×	•	6	**NGC 3226, 3227 Seyfert 1**, clear spiral galaxy
10292−4148	10 31 23.3 −42 03 41	×	×	×	×	×	×	×	×	×	×	×	6	**SGC 102912-4148.2 galaxy**,
10381−5704	10 40 09.0 −57 20 03	×	×	×	×	×	•	•	•	×	×	×	2	1 red star, some neb.
10406−6253	10 42 28.3 −63 09 39	×	×	×	×	×	•	•	•	×	×	×	3	*in DCld 289.0-03.8*, sev. red stars, some faint neb.
11507−6213	11 53 12.8 −62 30 17	×	×	×	×	×	•	•	•	×	×	×	7	nothing obvious
12190−6215	12 21 50.8 −62 31 42	×	×	×	×	×	•	•	•	×	×	×	7	nothing obvious
12196−6300	12 22 23.8 −63 17 14	×	×	×	×	×	•	•	•	×	×	×	3	*in vdB 57*, sev. red stars, neb.
12389−6147	12 41 53.4 −62 04 06	×	×	×	×	×	•	•	•	×	×	×	3	*in DCld 302.0+00.8*, sev. red stars, neb.
12391−6156	12 42 07.8 −62 13 14	×	×	×	×	×	•	•	•	×	×	×	7	nothing obvious
13168−6208	13 20 05.7 −62 24 02	×	×	×	×	×	•	•	•	×	×	×	7	nothing obvious
13224−5928	13 25 40.6 −59 43 42	×	×	×	×	×	•	•	•	×	×	×	1	**YSO**,*in DCld 307.3+02.9*,1 very red star, neb.
14047−6123	14 08 25.8 −61 37 40	×	×	×	×	×	•	•	•	×	×	×	7	nothing obvious
14188+7148	14 19 26.6 +71 35 15	×	×	×	•	•	×	×	×	•	×	•	6	**NGC 5607, Mrk 286 galaxy**, obvious galaxy
14375−6052	14 41 25.4 −61 05 12	×	×	×	×	×	•	•	•	×	×	×	7	nothing obvious
14454−4343	14 48 44.2 −43 55 41	×	×	×	×	×	•	•	•	×	×	×	6	**ESO 273-4 Seyfert 2**
14563−6301	15 00 24.9 −63 13 34	×	×	×	×	×	•	•	•	×	×	×	1	*in vdB 65*, 1 red star, neb.
15064−6429	15 10 40.9 −64 40 28	×	×	×	×	×	•	•	•	×	×	×	1	**NGC 5844, PK 317-5.1 PN** Plan. neb.
15365−5435	15 40 21.0 −54 45 00	×	×	×	×	×	×	•	•	×	×	×	1	red star with cometary neb.
15532−4210	15 56 42.5 −42 19 25	×	×	×	×	×	•	•	•	×	×	×	4	**HD 142527 HAeBe**
16017−3936	16 05 04.7 −39 45 03	×	×	×	×	×	•	•	•	×	×	×	7	*in BHR 126*, nothing obvious
16309−5758	16 35 13.0 −58 04 47	×	×	×	×	×	•	•	•	×	×	×	6	**ESO 137-34 Seyfert 2**
17199−3711	17 23 22.9 −37 13 47	×	×	×	×	×	•	•	•	×	×	×	7	nothing obvious
17340−3757	17 37 29.6 −37 59 22	×	×	×	×	×	•	•	•	×	×	×	1	v. red star, ext. emis. neb.
18018−2426	18 04 53.8 −24 26 40	×	×	×	•	•	•	•	•	•	×	•	1	**RAFGL 2059**, *in M8E region, by S25*, v. red star, emis. neb.
18064−2413	18 09 30.6 −24 12 33	×	×	×	•	•	•	•	•	•	•	•	3	**PK 6-2.1 PN mis-ID**, *by S29*, sev. stars, neb.
18361−0647	18 38 50.7 −06 44 53	×	×	×	•	•	•	•	×	×	×	×	7	*in L 495*, nothing obvious
18585−3701	19 01 55.3 −36 57 11	×	×	×	×	×	•	×	•	×	×	×	4	**R CrA HAeBe**, *in NGC 6729 dif. neb.*, v. lum. refl. neb.
19025+0739	19 04 60.0 +07 44 24	×	×	×	•	•	•	•	×	•	×	•	2	several red stars, no neb.
19050+0524	19 07 32.7 +05 29 41	×	×	×	•	•	×	×	×	•	×	•	2	*by S74*, sev. m. red stars, dark neb?
19111+0212	19 13 41.7 +02 17 39	×	×	×	×	×	×	×	×	×	×	×	4	**PK 37-3.3 symb**, bright star
19187+1556	19 20 58.2 +16 02 16	×	×	×	•	•	•	•	•	•	×	•	7	nothing obvious
19340+2228	19 36 09.6 +22 35 14	×	×	×	×	×	×	×	×	•	•	•	4	**HD 184961**, bright star
19348−0619	19 37 32.7 −06 13 05	×	×	×	•	•	•	•	•	×	×	×	6	probable galaxy with bright core
19365+2557	19 38 34.6 +26 04 47	×	×	×	•	•	×	×	×	•	•	•	2	1 red star, no neb, globule?
19520+2616	19 54 05.5 +26 24 28	×	×	×	•	•	×	×	×	•	•	•	5	some red stars
20024+3330	20 04 22.5 +33 38 58	×	×	×	•	•	×	×	×	•	•	•	1	**G070.7+01.2 (many IDs)**, Some controversy...
20049+3326	20 06 52.7 +33 34 46	×	×	×	•	•	×	×	×	•	•	•	5	*in LBN 162*, many red stars
20072+2720	20 09 20.1 +27 29 24	×	×	×	•	•	×	×	×	•	•	•	3	anon. dark cloud, v. red star, sev. red stars, neb.
20078+3528	20 09 44.7 +35 37 05	×	•	×	•	•	×	×	×	•	•	•	2	*in LBN 182*, diff. neb, sev. m. red stars
20172+3554	20 19 10.7 +36 03 54	×	×	×	•	•	×	×	×	•	•	•	2	1 v. red star, some m. red stars, no neb
20193+3448	20 21 18.7 +34 57 48	×	×	×	•	•	×	×	×	•	•	•	1	v. red star + neb.

• = data obtained; × = data not obtained

Table 1. (continued)

IRAS ID	RA (J2000) DEC	g'	r'	i'	g	r	V	R	I	J	H	K	ID	notes
20236+4058	20 25 27.8 +41 08 19	×	●	×	●	●	×	×	×	●	●	●	1	*in LBN 253*, v. red star + neb.
20337+4036	20 35 32.7 +40 46 33	×	●	×	●	●	×	×	×	●	●	●	1	*in LBN 271*, v. red star
20489+4410	20 50 43.2 +44 21 58	×	●	×	●	●	×	×	×	●	●	●	3	*in LBN 353*, lots of dark neb., refl neb, v. red stars
20496+4354	20 51 26.2 +44 05 22	×	●	×	●	●	×	×	×	●	●	●	3	*in LBN 343*, 2-3 v. red obj, refl. + emis. neb.
20582+7724	20 57 13.1 +77 35 46	×	●	×	●	●	×	×	×	●	●	●	1	*in L 1228*, dark neb., several red obj, neb
21004+7811	20 59 14.2 +78 23 00	×	●	×	●	●	×	×	×	●	●	●	3	**G82b 20**, dark neb, refl. neb, red stars
21351+5625	21 36 46.4 +56 38 56	×	×	×	●	●	×	×	×	●	●	●	5	**IC 1396**, red cluster
21485+5645	21 50 12.6 +56 59 23	×	×	×	●	●	×	×	×	●	●	●	5	**Trumpler 37**, red cluster
21569+5842	21 58 36.4 +58 57 08	×	×	×	●	●	×	×	×	●	●	●	1	*in L 1143*, v. red star, neb
22172+5549	22 19 09.0 +56 04 44	×	×	×	●	●	×	×	×	●	●	●	5	*in S132, LBN 473*, several red stars, lots of neb (emis?)
22206+6333	22 22 18.0 +63 48 51	×	×	×	●	●	×	×	×	●	●	●	2	*in L 1204*, some red stars
22299+6435	22 31 34.9 +64 50 46	×	×	×	●	●	×	×	×	●	●	●	7	*in LBN 520, by S150*, nothing obvious
23262+0314	23 28 47.0 +03 30 45	×	×	×	●	●	●	●	●	●	×	●	6	**NGC 7679 (galaxy pair)**, probable galaxy
23350+6413	23 37 24.5 +64 29 45	×	×	×	●	●	×	×	×	●	×	●	5	faint, red cluster
23395+6358	23 41 56.0 +64 15 09	×	×	×	●	●	×	×	×	●	●	●	1	a single v. red star

● = data obtained; × = data not obtained

Near-IR images of the Northern sources were taken with GRIM II, a near-IR imager and spectrograph which uses a 256^2 NICMOS-3 detector. The images were taken using the f/5 camera which gives a pixel scale of about 0.″48 with this detector. Images were obtained using a large number of short (1.2–10 sec) observations laid out in a dithering pattern to minimized the effects of bad pixels and to improve the total observed field-of-view. Analysis of the images requires the construction of a dark image and a flat-field image for each night. Since the scattered light contribution changes substantially during the course of a night, a template background must be constructed from a set of images taken over a short period of time. This background can then be subtracted from each of the dithered images before they are combined into a single mosaicked image.

Near-IR observations were made principally in J and K', but some observations were made with the H and K filters. The K and K' filters are generally similar, with the K' bandpass slightly bluer than K. We used only K standards and transformed the K' observations to K magnitudes. This step theoretically introduces some scatter, but given our relatively limited photometric accuracy, we are not sensitive to the difference between the two filters. We used only an airmass term and a linear $J-K$ color term for the calibrations. The scatter was large compared with the correction introduced by the color term. On the nights which were photometric, we used a variety of photometric standards from the Faint Standards list of the United Kingdom Infrared Telescope (UKIRT) to perform photometric calibration (Casali & Hawarden 1992). The zero points determined throughout the different nights were in good agreement with each other, at the 0.07 mag level. The major exception were those nights before the re-aluminization of the primary mirror in December 1996. In those observations, the zero points are about 0.5 mag brighter, consistent with the overall improvement in the throughput of the telescope observed after the re-aluminization process. A limitation of our calibration is the lack of very red standards. The target objects mostly have $J-K>1$ while all of the standards have $J-K<1$. The difference introduces a systematic error, but we believe the magnitude is small since the color term was less than a few percent. As a result of a limited number of calibration observations and internal scatter during photometric nights, the photometric calibrations are accurate to ~ 0.07 mag.

Optical observations of the Northern sources were performed with the Dual Imaging Spectrograph (DIS) in an imaging mode and with the imager SPIcam. DIS uses a dichroic to allow for simultaneous observations in a red and a blue channel. The dichroic transition is roughly 5350 Å, and the red and blue sides were imaged with a Thuan-Gunn r and g filter respectively. The blue side uses a SITe 512^2 CCD with 27 μm pixels while the red side uses a TI 800^2 CCD with 15 μm pixels. The resulting pixel scales are roughly 1.″1 for the blue chip and 0.″6 for the red chip. Photometric calibrations of the r and g images were performed using observations of Landolt (1992) standard stars with Thuan-Gunn photometry reported by Jørgensen (1994). Formal errors for the calibration are 0.05 mag for r and 0.04 mag for g.

The Seaver Prototype Imaging camera (SPIcam) uses a 2048^2 SITe CCD with 24 μm pixels. Images are normally read out in a 2×2 binned format, resulting in a plate scale of 0.″28. SPIcam has a filter wheel with 6 slots. For most of our observations with SPIcam, we used filters designed to match the Sloan Digital Sky Survey filter set. We denote these as g_*, r_*, and i_* in keeping with the recommendations of Krisciunas et al. (1998) since the final photometric system has not yet been defined. Photometric calibrations were performed using the observations of standard stars from Krisciunas et al. (1998). For the first set of observations performed with SPIcam, the filter wheel was not yet installed and only one filter could be used during the course of the night. For those observations, as marked, we used a filter designed for a separate project with approximately the same passband as r_*. These observations do not have a useful zero

Table 2. Log of APO 3.5m observations

Date	Camera	Filters	Conditions
96.08.12	DIS	r, g	non-photometric
96.11.13	DIS	r, g	non-photometric
97.11.19	DIS	r, g	photometric first half
96.08.20	GRIM	J, K'	non-photometric
96.10.02	GRIM	J, K'	non-photometric
97.01.29	GRIM	J, K'	photometric
97.05.14	GRIM	J, H, K'	photometric
97.11.19	GRIM	J, K	cirrus near end
97.12.05	GRIM	H	non-photometric
96.11.14	SPIcam	B_{45}	non-photometric
97.02.02	SPIcam	g_*, i_*	non-photometric
97.11.23	SPIcam	g_*, i_*	non-photometric
97.12.05	SPIcam	g_*, i_*	photometric

point calibration and are therefore useful only for relative colors and for the detection of filaments bright in Hα.

5. The catalog

Table 1 lists all of our candidate transitional YSOs identified on the basis of IRAS colors and the morphology in the DSS. In this table, we have listed the filters which have been used to image each of the targets, as well as the IRAS source number and the J2000 coordinates of each object, derived from the IRAS Point Source Catalog. For each filter listed, a dot indicates that observations have been performed while an $\times$ indicates no observations. We also have included our category IDs for each source, as discussed above, as well as a short description of the optical / near-IR appearance of the source. We have also included cross-identifications in cases where specific identifications have been made for the objects, using the Simbad database for initial cross-references. In the cross identification, objects which are alternative names for the same object are listed with bold print. As an example, IRAS 05293+1701 is the bright star HD 36408. We have also made notations where the IRAS source is in the vicinity or contained within a larger object, such as a Lynds Bright Nebula (LBN), a Lynds Dark Nebula (Lnnn), or a Sharpless H II region (Snnn). These notations are made using italic print and include a preposition "in" or "by".

We also present in electronic form optical and near-IR images for each source. For the optical images, we have selected the best image near Johnson V: the g images for the DIS data and g_* images for the SPIcam data. If neither image was available for a given source, we used one of the other optical filter images. For the near-IR images, we present the best J and K band image of each source.

We have also generated high-resolution 60 μm IRAS images for each of the sources in the catalog. These images were produced using the HIRAS image restoration technique (Bontekoe et al. 1994), which is essentially an extension of maximum entropy. The HIRAS images cover a large field ($32' \times 32'$) compared to the optical and near-IR images. We include the full HIRAS image in the electronic catalog. In the optical and near-IR images, the 1σ confidence location of the IRAS source is marked with an error bar or ellipse and contours from the HIRAS image are overlayed.

In the process of generating the HIRAS images, we have inspected the information in the raw IRAS snips. For IRAS 06584−0852 a glitch is present in the IRAS positional data. For this source, the orientation of the error ellipse listed in the IRAS Point Source Catalogue is also not oriented perpendicular to the average IRAS scan direction. Therefore we conclude that the orientation of the error ellipse quoted in the Point Source Catalogue is probably incorrect. We estimate the true orientation to be $100 \pm 10^\circ$.

The complete set of images is available electronically for each source from the Centre de Données astronomique de Strasbourg (CDS). We also present the results for a single source, IRAS 03507+3801 in Fig. 1. Notice that this source is an excellent example of a probable YSO in transition. This source is significantly reddened, and is surrounded by an apparent reflection nebula. Several pieces of evidence suggest the nebula is a reflection nebula: the relatively blue color of the nebula, the absence of strong emission in g (ie, Hα emission), and the generally smooth nature (no tendrils of ionization fronts typically seen in emission nebulae) all support this suggestion. The fact that the morphology of the nebula changes shape with wavelength is reminiscent of the reflection nebula of IRAS 05327+3404 (Holoea) and may point to varying amounts of obscuration between the central star and the nebula, as expected in disk systems.

6. Results

Our major goal was to identify transitional YSOs, using IRAS 05327+3404 (Holoea) as a guide. In this case, we expect to find a single, significantly reddened stellar object with an associated reflection nebula. It is possible to distinguish reflection and emission nebulae on the basis of wide-band images: reflection nebulae are relatively blue and in general have comparable flux in a variety of wide-band images. Emission nebulae, on the other hand, have principally Balmer emission and therefore are much more evident in the wide-band images which include Hα (r and r_*) and are much fainter in other bands. Emission nebulae are likely to be seen with higher mass YSOs (Herbig Ae/Be stars) or with Planetary Nebulae, a likely contaminant. Reflection nebulae, particularly bipolar reflection nebulae, are typically seen with heavily embedded YSOs (see Staude & Elsässer 1993), although they may also be found in the vicinity of Herbig Ae/Be stars.

We present our identifications of each of the objects observed in Table 1. We have defined 7 categories of objects seen in the optical and IR images:

1. A likely transitional YSO: A single moderately-bright, very-red stellar object with extensive associated reflection nebulosity. (28 objects)
2. A possible transitional YSO: a moderately red stellar object with weak nebulosity or a significantly red object with no nebulosity. (22 objects)

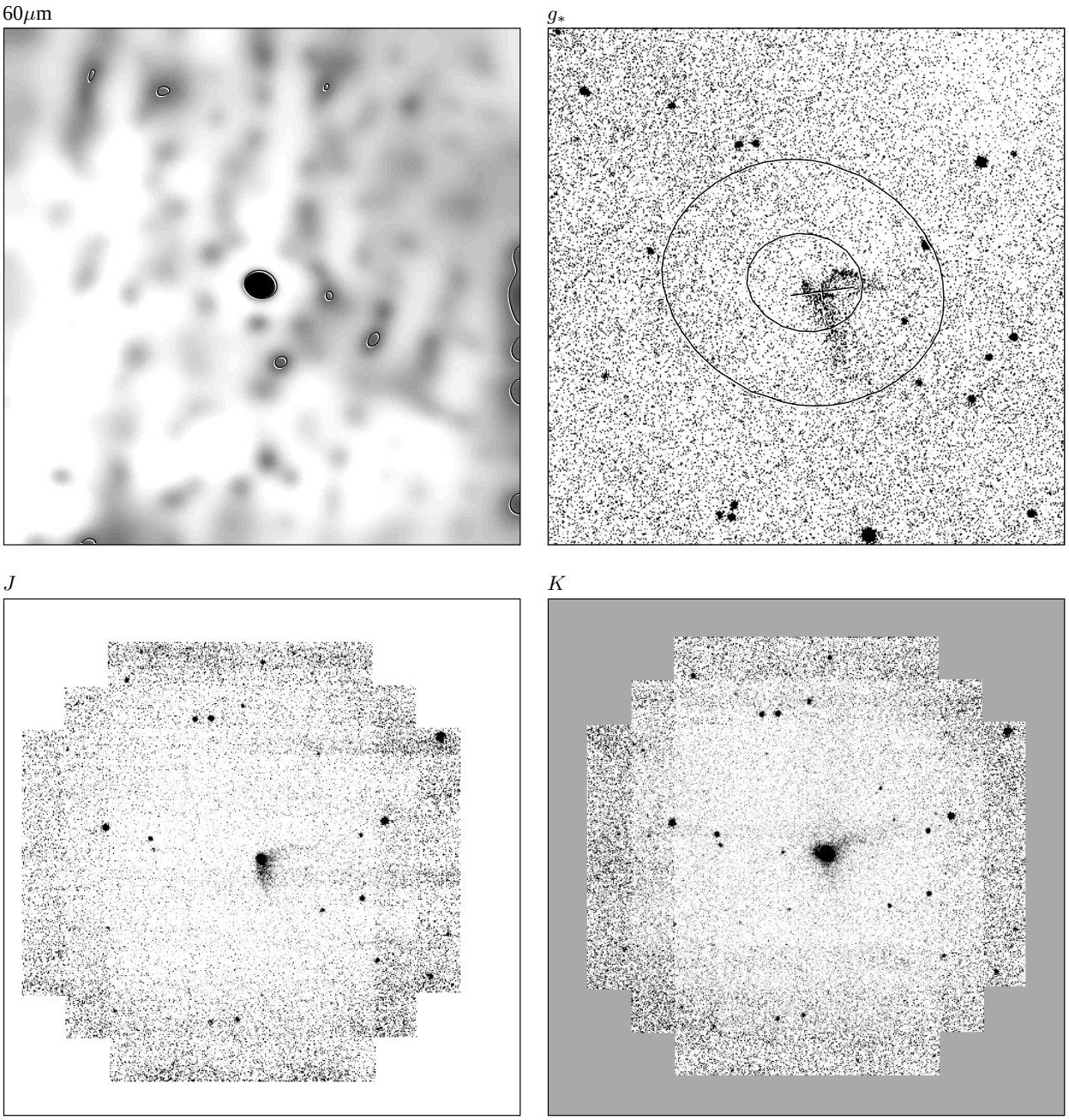

Fig. 1. Example of catalog images – IRAS 03507+3801. Shown are the HIRAS 60 μm image and the APO images in the g_*, J and K bands. The contours in the HIRAS image and in the g_* band image indicate the HIRAS 60 μm flux levels. The contours are drawn at 0.5 and 20σ above the background level, where σ is the standard deviation in background region. The error bar shows the size and orientation of the position give by the IRAS Point Source Catalogue. All images have North up, East left. The HIRAS image is $32' \times 32'$, while the other three images are each $4' \times 4'$.

3. A YSO group: Several very red objects, usually with extended nebulosity. No single object stands out. (21 objects)
4. Bright star. (7 objects)
5. A cluster of stars: usually a red cluster with no single very red star. (18 objects)
6. A galaxy. (11 objects)
7. nothing: no object stands out, and no object can be associated with any of the other classes. (18 objects)

The first three of these categories are likely to include the isolated YSOs or groups of YSOs. The first two probably include the transitional YSOs which we were interested in finding, though objects in the second category are somewhat weaker candidates. Objects in the third category are also likely to be YSOs, but it is less likely in these cases that the YSOs are transitional in the sense we have defined above. Although a single flat-spectrum IRAS source is identified with these groups, it is prob-

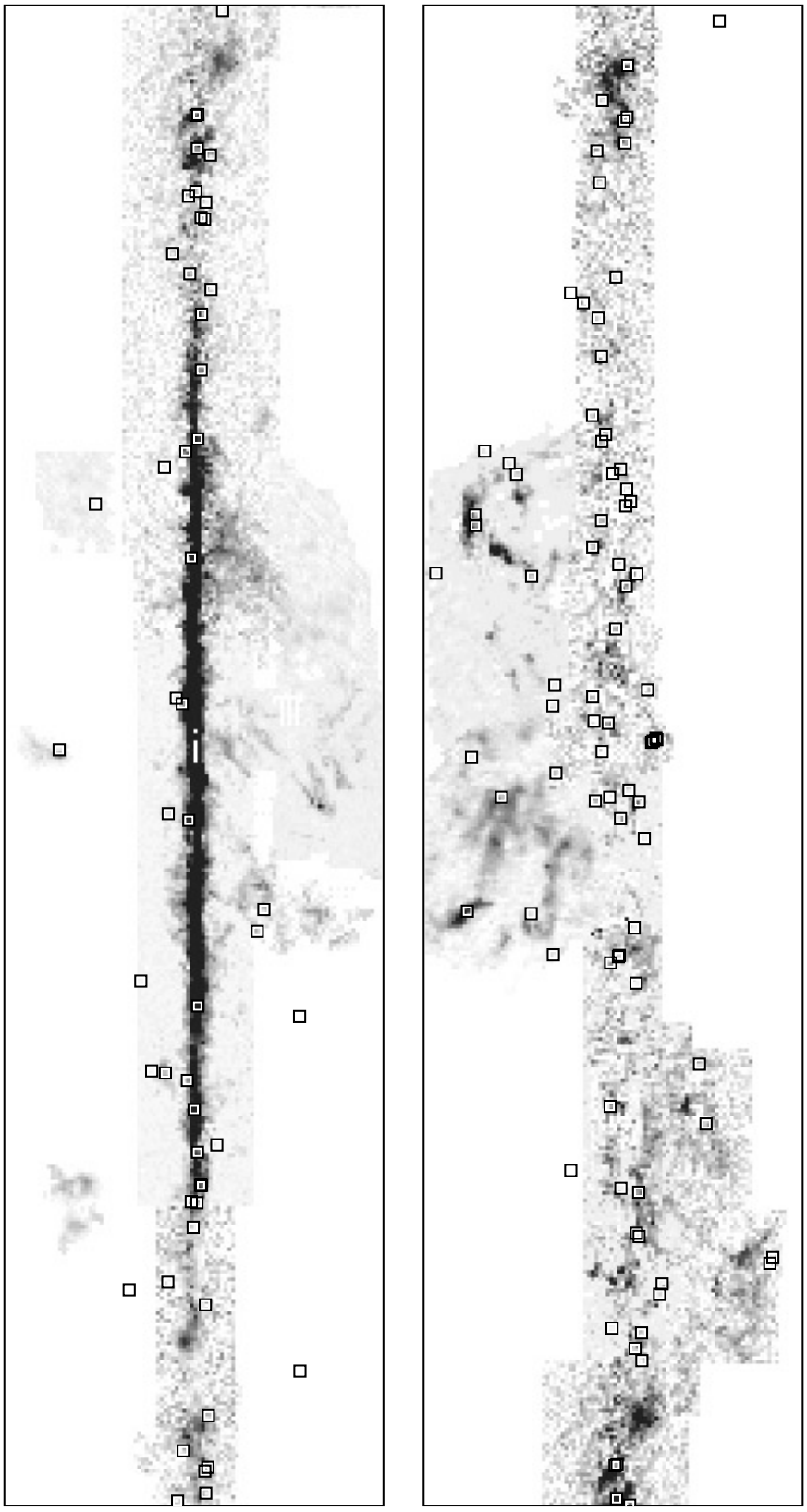

Fig. 2. Greyscale CO Maps of the inner (left) and outer (right) Galactic plane (Dame et al. 1987) with the locations of our Transitional YSOs marked with boxes. The fact that essentially of of our candidates lie close to the plane or in areas of strong CO emission implies that the bulk of our objects are a young population. These images are $45^\circ \times 180^\circ$.

able that the emission is due to more than one source. In this case, the flat-spectrum may be due to the overlap of emission from different sources and only more detailed studies in the mid-IR, far-IR, or submillimeter may identify true transitional sources among these object. Objects in category 4 are mostly likely too bright optically to be considered transitional, and may be good

candidate Herbig Ae/Be stars; indeed some are already identified as such. The objects IRAS 05017+2639 (HD 32509), IRAS 05111+3244 (HD 241699) and IRAS 06041+3012 (MWC 790) may be previously unknown HAeBe candidates and deserve further study. Category 5 objects are likely to be young, embedded clusters, which may contain YSOs of a range of evolutionary states. However, the flat IRAS spectra of these sources is, like category 3, likely to be due to the superposition of several different sources. The 11 objects in category 6 are all clearly associated with objects which are obviously galaxies, some of which have been identified in a search for galaxies in the Zone of Avoidance (Weinberger et al. 1995). Many of these are likely to be Seyfert galaxies which are known to have flat IRAS spectra. Finally, for group 7, a small number of objects had no obvious optical or near-IR counterparts to the IRAS source. In several of these cases, the HIRAS image is very crowded. It is possible in these cases that the flat IRAS spectrum may be the result of IRAS source confusion.

Fig 2 shows the distribution of the transitional YSO candidates relative to the Galactic CO distribution. Each object is overlayed on the CO map of Dame et al. (1987). The vast majority of the objects in the catalog are found in the general vicinity of CO clouds and generally near other signs of active star formation. This association, along with the general tendency for these objects to lie near evidence of star formation (see Table 1), lends credence to our claim that the bulk of these sources are young stellar objects. Except for the 11 sources which are clearly associated with galaxies, essentially all of the sources lie in the Galactic plane or in the CO spurs. We conclude that the contamination by Planetary Nebulae is insignificant, though a small number of specific objects may possibly be PNe.

7. Conclusions

We have surveyed a total of 125 candidate transitional YSOs. Our goal was to find isolated YSOs with flat IRAS emission, indicating a relatively young age, but with a visible central star, indicating the star is at the transition between the embedded and exposed phases of early stellar evolution. In this task, we have been very successful. Of the 125 objects, 28 are very strong candidates (category 1) to fit this description, while another 22 are possible (category 2). There are also 21 objects for which a group of several stars is visible, one or more of which may be transitional YSOs (category 3). In this case, however, follow-up observations in the mid and far IR will be needed to determine which of the sources contribute to the strong 60 μm emission and if any specific one of these sources can be considered transitional. Two other classes of objects are related to the YSOs of interest, but do not fit the group we are interested in. First, the objects for which a very bright star is seen are likely to be Herbig Ae/Be stars which have very large, or very cool, circumstellar disks. In these cases, the star has clearly been exposed, since it is strongly detected in the optical, so it does not fit our description of a transitional object. There are 7 of these stars in our sample of which three were not previously considered HAeBe candidates. The other group are the reddened clusters. These are likely to be young clusters either recently formed or still in the process of forming. The flat far-IR emission is probably due to the superposition of many sources. While interesting in themselves, these sources will not make for simple study of an early, transitional star. There are 18 embedded clusters in the sample. Finally, there are 11 sources associated with galaxies. One of these appears to be a giant association or H II region in the galaxy IC 342. The other 10 appear to be the cores of Seyfert galaxies, which are known to have IRAS colors similar to our selections. The bulk of our candidates sources lie in the plane of the Galaxy, near areas of recent star formation, lending support to our expectation that most of these are young stars. The complete set of images is available electronically for each source from the Centre de Données astronomique de Strasbourg (CDS - `http://cdsweb.u-strasbg.fr/CDS.html`).

Acknowledgements. EAM acknowledges support by the Netherlands Foundation for Research in Astronomy (ASTRON) with financial aid from the Netherlands Organization for Scientific Research (NWO) under contract number 782-376-011. Support for EAM was also provided by NASA through grant number GO-06459.01-95A from the Space Telescope Science Institute, which is operated by the Association of Universities for research in Astronomy, Inc., under NASA contract NAS5-26555. LBFMW acknowledges financial support through a NWO *Pionier* grant. MvdA acknowledges financial support from NWO grant 614.41.003. The IRAS data were obtained using the IRAS data base server of the Space Research Organisation of the Netherlands (SRON) and the Dutch Expertise Centre for Astronomical Data Processing funded by the Netherlands Organisation for Scientific Research (NWO). We gratefully thank Do Kester and Romke Bontekoe for use of the IRAS-GIPSY system. The IRAS data base server project was also partly funded through the Air Force Office of Scientific Research, grants AFOSR 86-0140 and AFOSR 89-0320. This article uses data from the Digitized Sky Survey, based on photographic data of the National Geographic Society – Palomar Observatory Sky Survey (NGS-POSS) obtained using the Oschin Telescope on Palomar Mountain. The NGS-POSS was funded by a grant from the National Geographic Society to the California Institute of Technology. The plates were processed into the present compressed digital form with their permission. The Digitized Sky Survey was produced at the Space Telescope Science Institute under US Government grant NAG W-2166.

References

Adams F.C., Shu F.H., 1985, ApJ 296, 655
Adams F.C., Shu F.H., 1986, ApJ 308, 836
Adams F.C., Lada C.J., Shu F.H., 1987, ApJ 312, 788
Batalha C.C., Basri G., 1993, ApJ 412, 363
Beckwith S.V., Sargent A.J., Koresko C.D., Weintraub D.A., 1989, ApJ 343, 393
Bontekoe Tj.R., Koper E., Kester D.J.M., 1994, A&A 284, 1037
Campbell B., Persson S.E., Matthews K., 1989, AJ 98, 643
Casali M.M., Hawarden T.G., 1992, JCMT-UKIRT Newsletter 3, 33
Chen H., Bally J., O'Dell C.R, et al., 1998, ApJ 492, L173
Cohen M., Kuhi L.V., 1979, ApJS 41, 743
Cudworth K.M., Herbig G.H., 1979, AJ 84, 548
Dame T.M., Ungerechts H., Cohen R.S., et al., 1987, ApJ 322, 706
Fukui Y., Iwata T., Mizuna A., Bally J., Lane A.P., 1993, In: Levy E.H., Lunine J.I. (eds.) Protostars and Planets III, University of Arizona Press, p. 603

Henyey L.G., LeLevier R., Levee R.D., 1955, PASP 67, 154
Herbig A.G., 1960, ApJS 4, 337
IRAS Point Source Catalogue, 1985, US Government Publication Office
Jørgensen I., 1994, PASP 106, 967
Joy A.H., 1945, ApJ 102, 168
Krisciunas K., Margon B., Szkody P., 1998, PASP 110, 753
Kuhi L.V., 1964, ApJ 140, 1409
Lada C.J., Wilking B.A., 1984, ApJ 287, 610
Landolt A.U., 1992, AJ 104, 340
Luyten W.J., 1971, The Hyades. Univ. Minnesota Press, Minneapolis
Magnier E.A., Waters L.B.F.M., Kuan Y.-J., et al., 1996, A&A 305, 936 (Paper I)
McCaughrean M.J., O'Dell C.R., 1996, AJ 111, 1977
Mundt R., 1984, ApJ 280, 749
Myers P.C., Benson P.J., 1983, ApJ 266, 309
Norman C., Silk J., 1979, ApJ 228, 197
Persson S.E., Campbell B., 1987, AJ 94, 416
Prusti T., Adorf H.-M., Meurs E.J.A., 1992, A&A 261, 685
Rodriguez L.F., Moran J.M., Ho P.T.P., Gottlieb E.W., 1980, ApJ 224, 845
Schwartz R.D., 1978, ApJ 223, 884
Shu F.H., 1977, ApJ 214, 488
Snell R.L., Loren R.B., Plambeck R.L., 1980, ApJ 239, L17
Stahler S.W., 1983, ApJ 274, 822
Stahler S.W., 1988a, ApJ 332, 804
Stahler S.W., 1988b, PASP 100, 1474
Stahler S.W., 1994, PASP 106, 337
Staude H.J., Elsässer H., 1993, A&AR 5, 165
Walker M.F., 1956, ApJS 2, 365
Weinberger R., Saurer W., Seeberger R., 1995, A&AS 110, 269